Journal of Alloys and Compounds 503 (2010) 111–117

Contents lists available at ScienceDirect

Journal of Alloys and Compounds

journal homepage: www.elsevier.com/locate/jallcom

Influence of sintering temperature on the structural, magnetic and dielectric properties of $Ni_{0.8}Zn_{0.2}Fe_2O_4$ synthesized by co-precipitation route

Tania Jahanbin[a,*], Mansor Hashim[a,b], Khamirul Amin Matori[a], Samaila Bawa Waje[b]

[a] Department of Physics, Faculty of Science, Universiti Putra Malaysia, 43400 UPM Serdang, Selangor, Malaysia
[b] Advance Materials and Nanotechnology Laboratory, Institute of Advanced Material Technology, Universiti Putra Malaysia, 43400 UPM Serdang, Selangor, Malaysia

ARTICLE INFO

Article history:
Received 9 January 2010
Received in revised form 22 April 2010
Accepted 28 April 2010
Available online 6 May 2010

Keywords:
Co-precipitation
Permeability
Permittivity

ABSTRACT

The polycrystalline Ni–Zn ferrite powder with the chemical formula $Ni_{0.8}Zn_{0.2}Fe_2O_4$ has been synthesized using co-precipitation route. The toroidal and pellet form samples were sintered at various temperatures from 700 to 1300 °C/5 h in steps of 200 °C. The structures of samples were studied by means of X-ray diffraction (XRD), scanning electron microscopy (SEM) and the energy dispersive X-ray spectroscopy (EDXS). The magnetic and dielectric measurements were carried out using a vibrating sample magnetometer (VSM) and the impedance analyzer, respectively. The highest density of 4.48 g cm^{-3} was obtained for the sample sintered at 1300 °C. It was found that the initial permeability increased from 4 to 17 and the RLF was in the order of 10^{-3} to 10^{-4} in the frequency range of 1.0 MHz to 1.0 GHz. The dielectric constant and dielectric loss were lower compared to the reported values for conventional solid state technique. The electrical resistivity is in the order of 10^8 Ω cm. Therefore, low relative loss factor and high resistivity make these ferrites particularly useful as inductor and transformer materials for high frequency applications.

1. Introduction

Nickel–zinc ferrite is a soft ferrite with low magnetic coercivity and high resistivity values [1]. The high electrical resistivity and good magnetic properties make this ferrite an excellent core material for power transformers in electronic and telecommunication applications [2,3].

In the Ni–Zn ferrite, the electrical and magnetic properties are highly sensitive to the stoichiometric composition, heat treatment and preparation method. It is well known that nickel–zinc ferrites are superior to most other ferrites for use at high frequency because of their high electrical resistivity and low energy loss. However, many of the findings on their excellent properties were obtained using samples produced by the conventional ceramic processing technique. This technique has been, for several decades, the most common method for preparation of ferrites. However, some of its inherent drawbacks are poor compositional control, chemical inhomogeneity, coarser grain size and introduction of impurities during grinding [4]. Since wet chemical methods are widely believed to be able to overcome these drawbacks, it is envisaged that nickel–zinc ferrites with better properties can be obtained using these methods.

Nowadays, more efforts are being carried out to develop higher electric–magnetic properties and low-power loss materials in the MHz frequency region. Thus, the research activity is directed to produce better stoichiometry and reproducible ferrites which involve heat treatment at lower temperatures and shorter duration [5]. Specifically, the work is aimed evaluating the structure, morphology and magnetic properties of the Ni–Zn ferrite prepared by co-precipitation, with the view to increase the operational frequency of the resulting ferrite samples.

2. Experimental methods

2.1. Synthesis

Nanocrystalline nickel–zinc ferrite was synthesized using the co-precipitation route. The nitrates of nickel, zinc and ferric (99.99%) were used as raw materials. Ammonia hydroxide (25%) was used as a base. Its salts are volatile on subsequent heating and hence impurity of the isolated powders due to the precipitating reagent can be avoided. The co-precipitation Ni–Zn ferrite, $Ni_{0.8}Zn_{0.2}Fe_2O_4$, was prepared via co-precipitation according to Eq. (1). The metal nitrates were separately dissolved in distilled water using electronic stirrer at 300 rpm to form a clear solution. The resulting solution was mixed together and stirred for 3 h to give the homogeneous mixture. The precipitating reagent was added drop-wise into metal solutions, contained in a beaker, with constant stirring until a pH of 9 is reached. This is to assure the complete precipitation [6]. The reaction temperature was kept at 85 °C for 45 min.

$$0.8Zn(NO_3)_2{\cdot}6H_2O + 0.2Ni(NO_3)_2{\cdot}6H_2O + 2Fe(NO_3)_3{\cdot}9H_2O + 8NH_4(OH) \rightarrow Ni_{0.8}Zn_{0.2}Fe_2(OH)_8 + 8NH_4NO_3 + 24H_2O \quad (1)$$

The reaction was afterwards stopped and the resulting precipitates washed with deionised water, and dried in an electric oven at a temperature of 110 °C for

* Corresponding author. Tel.: +60 178863913.
E-mail address: Tanya.jahanbin@yahoo.com (T. Jahanbin).

0925-8388/$ – see front matter © 2010 Elsevier B.V. All rights reserved.
doi:10.1016/j.jallcom.2010.04.212

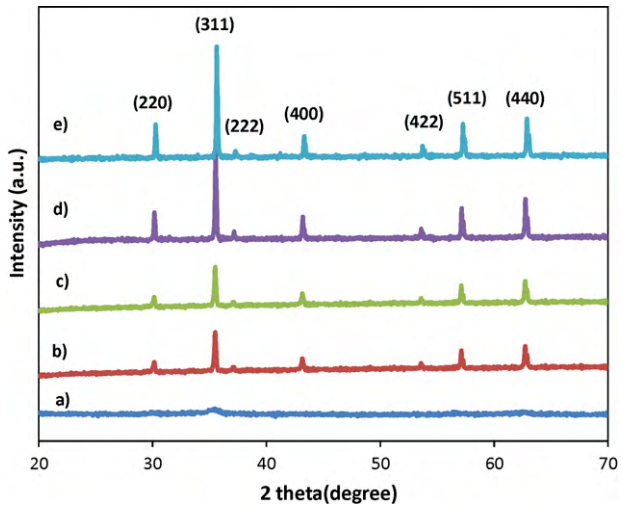

Fig. 1. The XRD patterns of $Ni_{0.8}Zn_{0.2}Fe_2O_4$ sintered at (a) before sintering, (b) 700 °C, (c) 900 °C, (d) 1100 °C, and (e) 1300 °C prepared via the co-precipitation technique.

overnight to remove water contents. The dried powder was mixed homogeneously in a cleaned agate mortar and pestle. The powder was formed as pellet/toroid shapes by using hydraulic press, applying a load of 60 kN for 5 min in each case. Finally, the samples were sintered at different temperatures.

2.2. Characterization

Structural changes of powder particles were studied by X-ray diffraction (XRD) in a Philips X'PERT MPD diffractometer using filtered Cu Kα radiation (λ = 0.1542 nm) obtained in the 2θ range 20–70° using a scan step of (2θ) = 0.0330° with 5 s per step as the counting. The microstructure of the sintered sample was examined by scanning electron microscope (SEM). The Archimedes principle was used to determine the density of the sintered toroids. Both the initial permeability, μ_i, and loss factor, RLF, were evaluated using the impedance analyzer model (HP 4291B) in the frequency range 1 MHz to 1 GHz on the toroidal ferrite. Dielectric measurements such as dielectric constant, ε', and loss tangent, ε'', were carried out in the frequency range 1 MHz to 1 GHz on pellets form of samples at an operating voltage of 12 V using impedance analyzer (HP 4291B). The resistivity of sintered Ni–Zn ferrite was calculated by measuring an average of electrical resistance of toroidal samples, coated with a silver conductive paint and connected to the HP 34401A multi-meter. The hysteresis loop parameters were measured at room temperature by a vibrating sample magnetometer (VSM) in the field of 15 kOe.

3. Results and discussion

3.1. Structural characteristics measurements

The X-ray diffraction patterns of Ni–Zn ferrites ($Ni_{0.8}Zn_{0.2}Fe_2O_4$) prepared by co-precipitation method before sintering and sintered at different temperatures are shown in Fig. 1. The XRD patterns confirm the formation of the single-phase cubic spinel structure after sintering. During sintering the zinc diffuses into the iron oxide lattice, due to the low melting point of Zn, followed by diffusion of nickel which leads to produce spinel Ni–Zn ferrite. Referring to Fig. 1, there is no extra lines corresponding to any other crystallographic phase or unreacted ingredient. All peaks observed match well with those of Ni–Zn ferrites reported earlier [7].

The lattice parameters of the Ni–Zn ferrite sintered at different temperatures calculated from the (3 1 1) diffraction peak are listed in Table 1. The lattice constant of the samples was determined using the relation [8]:

$$a_0 = d_{h\,k\,l}(h^2 + k^2 + l^2)^{1/2} \quad (2)$$

The lattice parameter depends upon the composition and sintering temperature. As shown in Table 1 the lattice constant a_0 increases as the sintering temperature increased. The lattice expansion may be attributed to the reduction of Fe^{3+} and formation of Fe^{2+} ions while ionic radius of the Fe^{2+} (0.77 Å) is larger than the Fe^{3+} (0.63 Å). The lattice parameters, a_0, for the sintered samples are found to be in the range 8.356–8.365 Å with the uncertainty $\pm 1.6 \times 10^{-3}$ Å. These values are in a good agreement with those reported earlier [9].

Furthermore, Table 1 shows the bulk density and porosity of sintered Ni–Zn ferrite of composition $Ni_{0.8}Zn_{0.2}Fe_2O_4$ at various temperatures. It is observed that the bulk density increases as sintering temperatures increase. The obtained density which is between 4.99 and 5.1 g cm^{-3} is lower than that produced by the conventional route [7,10]. The total pores are directly related to the density. Therefore, the higher heat treatment and longer duration will remove pore contents. Porosity of the order of 14–24% is obtained for Ni–Zn ferrite of composition $Ni_{0.8}Zn_{0.2}Fe_2O_4$ sintered at various temperatures. The typical porosity which has been reported for ferrites is in the range 7–25% [11]. The sintered density obtained is higher than that of Ni–Zn ferrites prepared by flash combustion technique in normal heating [12].

3.2. Morphology (SEM)

The microstructure plays an important role in realizing many application-oriented ferrite properties. The SEM micrographs were taken to understand the microstructure of the prepared $Ni_{0.8}Zn_{0.2}Fe_2O_4$. The average grain size was determined using the relation [13]:

$$G_a = \frac{0.5L}{MN} \quad (3)$$

where L is the total test line length; M the magnification; N is the total number of intercepts. As shown in Fig. 2 and Table 2, grain sizes increase with sintering temperature. Samples sintered at 700 °C possess comparatively very small grains less than 1 μm while samples sintered at 1300 °C possess much larger grains. The higher grain size for the sample sintered at 1300 °C may be attributed to the formation of Fe^{2+} ions, which accelerate the growth rate of the grains [14,15]. It is observed that grain size of the samples under investigation is smaller than that prepared by ceramic method [16].

As illustrated in Fig. 2a, the microstructure of sample sintered at 700 °C shows that the grain boundaries are not completely formed due to the low sintering temperature. There are combinations of the neck and grain boundary. Neck is the solid bridge, which was formed during heating of precipitated powders. The porosity of ceramic samples results from two sources, intra-granular and inter-granular porosities [17]. Thus, the total porosity is the sum P_{intra} and P_{inter}. From Fig. 2, most of the porosity is inter-granular. However, in Fig. 2d, the grain growth increases dramatically and the grain boundaries become thinner which makes distinguishing between them is difficult. Generally, the grain growth is normal and

Table 1
The physical properties of $Ni_{0.8}Zn_{0.2}Fe_2O_4$ sintered at various temperatures.

Sintering temperature (°C)	Experimental density (g cm^{-3})	Porosity (%)	Lattice constant, a_0 (Å)
700	3.47	24	$8.356 \pm 1.6 \times 10^{-3}$
900	4.01	21	$8.358 \pm 1.6 \times 10^{-3}$
1100	4.19	18	$8.361 \pm 1.6 \times 10^{-3}$
1300	4.48	14	$8.365 \pm 1.6 \times 10^{-3}$

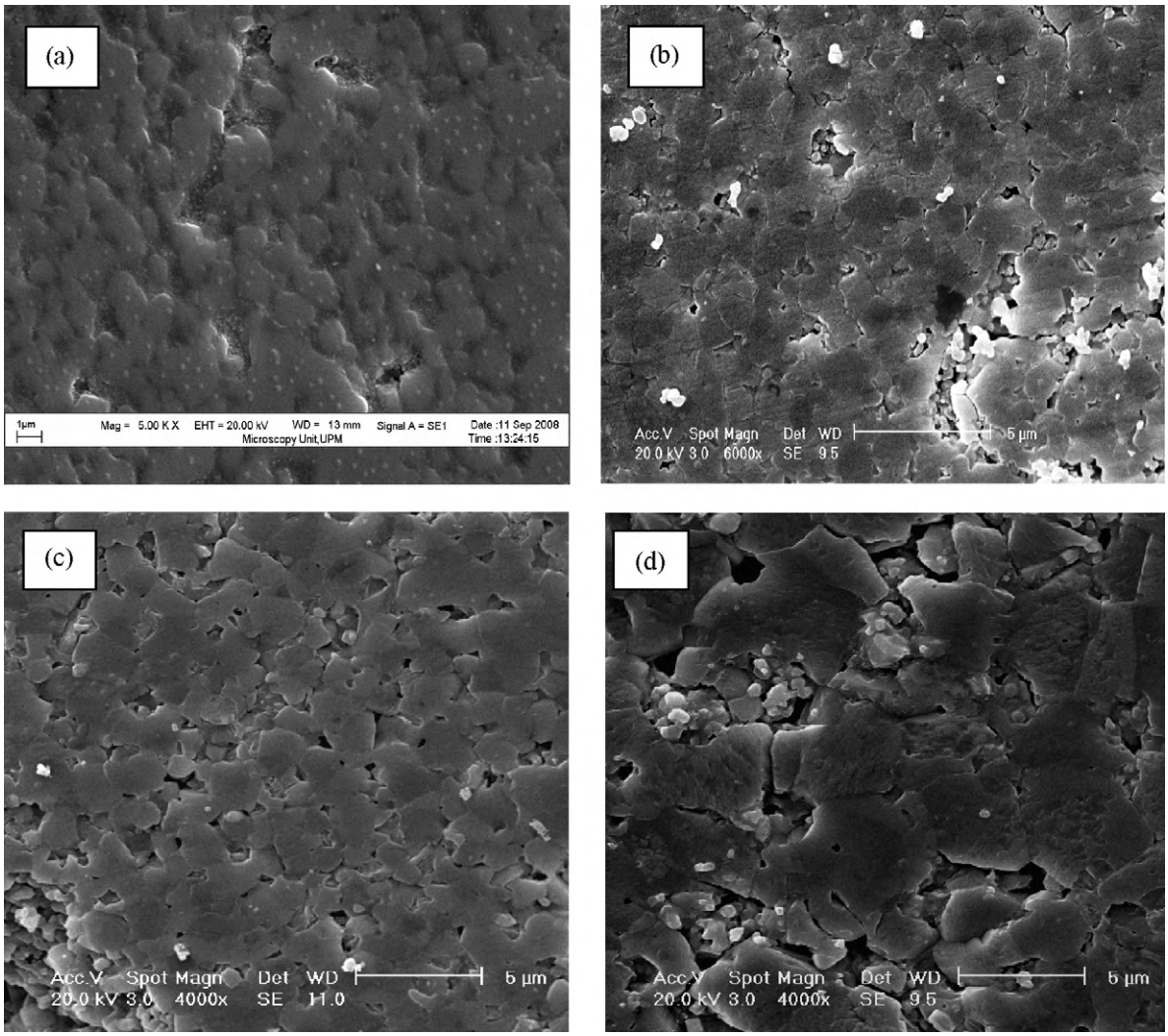

Fig. 2. SEM of Ni–Zn ferrites sintered at (a) 700 °C, (b) 900 °C, (c) 1100 °C, and (d) 1300 °C.

Table 2
Average grain size and resistivity of the $Ni_{0.8}Zn_{0.2}Fe_2O_4$ sintered at different temperatures.

Sintering temperature (°C)	Average grain size (μm)	Resistivity (Ω cm)
700	0.3	7.2×10^8
900	1.2	6.3×10^8
1100	2.1	5.4×10^8
1300	3.4	3.7×10^8

most of the grains grow pretty much at the same time and same rate.

Chemical composition analyses through EDXS were also carried out on the sample sintered at 700 and 1300 °C. The energy dispersive X-ray spectroscopy (EDXS) results can confirm the stoichiometry of the samples without the impurity in the sintered samples as shown in Fig. 3. The compositions of the samples obtained by EDXS analysis correspond to the expected chemical formula $Ni_{0.8}Zn_{0.2}Fe_2O_4$ are listed in Table 3. As listed in Table 3, the zinc volatilization takes place at 1300 °C.

3.3. DC electrical resistivity

The resistivity of the ferrite in general, depends on the density, porosity, grain size and chemical composition of the samples. In the present investigation, the DC resistivity of $Ni_{0.8}Zn_{0.2}Fe_2O_4$ sintered at various temperatures is listed in Table 2. It is observed that the resistivity of ferrite prepared under investigation is higher than reported values of resistivity of ferrite prepared by ceramic [18]. Resistivity values of the order $\geq 10^8$ Ω cm are obtained which are much higher than those of the reported values. This is attributed to the small size of grains as mentioned in Table 2. The samples with small grains contain a great number of grain boundaries. The grain boundary acts as a barrier to flow of electrons resulting in increased resistivity [19]. On the other hand, the main mechanism of conductivity in ferrites is electron hopping between the divalent and trivalent Fe ions, $Fe^{2+} \leftrightarrow Fe^{3+}$, in the spinel lattice [20]. The oxidation process of the smaller grain size is fast thus reducing the probability of Fe^{2+} ions [21]. Consequently, the resistivity increases. These are the reasons for the sample with small grain size exhibits the higher resistivity. It has been found from Fig. 4 that there is a reduction in resistivity for Ni–Zn ferrite with increase of sintering temperature. A similar trend was also reported by Naik and Powar [18] and Jain et

Table 3
The composition of $Ni_{0.8}Zn_{0.2}Fe_2O_4$ at various temperatures.

Sample ($Ni_{0.8}Zn_{0.2}Fe_2O_4$)	Elemental composition (wt%)			
	Nickel	Zinc	Iron	Oxygen
Sintered at 700 °C	19.50	5.28	48.90	26.32
Sintered at 1300 °C	19.28	4.54	48.78	27.4

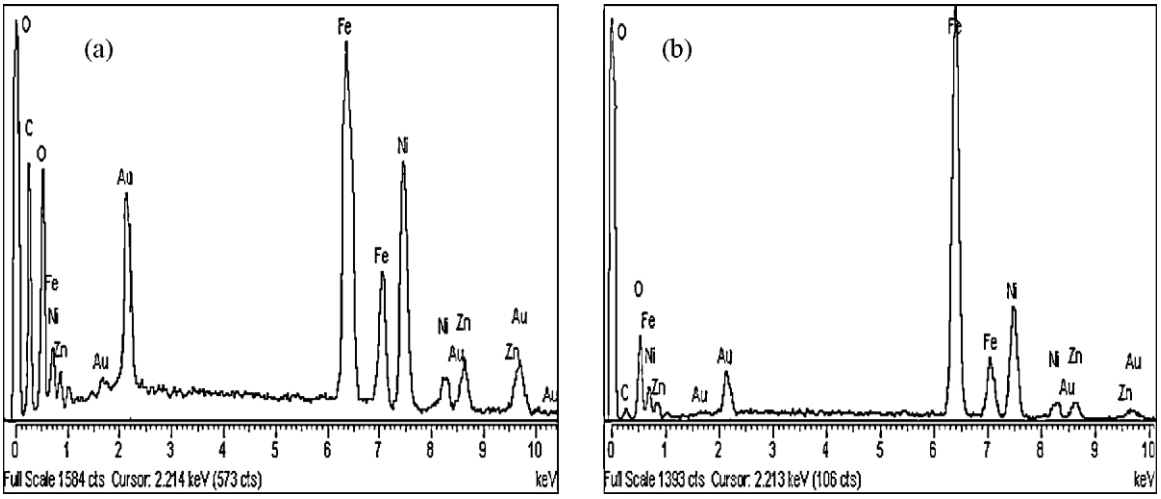

Fig. 3. The EDXS spectrum of $Ni_{0.8}Zn_{0.2}Fe_2O_4$ pellets sintered at (a) 700 °C and (b) 1300 °C.

al. [22]. The reduction in resistivity with increase of sintering temperature has been attributed to the increase of Fe^{2+} ions. During heating, the electron hopping between $Fe^{3+} \leftrightarrow Fe^{2+}$ increases, due to the zinc loss which causes increasing the formation of Fe^{2+} ions at higher sintering temperatures. This causes an increase of the conductivity, inversely decreasing the resistivity. Also the reduction of resistivity with increase of sintering temperature can be related to the reduced porosity, increased grain size and increased density which were obtained at higher temperature.

3.4. Dielectric behaviour

The dielectric properties of Ni–Zn ferrites were studied in the frequency range from 1 MHz to 1 GHz at room temperature. Fig. 5 shows variations of the dielectric constant as the function of frequency at room temperature (≈25 °C) for $Ni_{0.8}Zn_{0.2}Fe_2O_4$ sintered at various temperatures. Obviously, the dielectric constant increases with sintering temperature. The maximum value of the dielectric constant is obtained at 1.0 MHz for all samples. The variation of dielectric constant is not too much except for the sample sintered at 1300 °C, which comparatively has higher values of the dielectric constant.

The dielectric constant decreases with increase in frequency for all samples as shown in Fig. 5. The decrease is rapid at lower frequencies and slower at higher frequencies. The decrease in dielectric constant with increase in frequency is a normal dielectric behaviour which is also observed by several other investigations [12,23,24]. This treatment of ferromagnetic material may be due to the interfacial polarization that is predicted by Maxwell and Wagner. According to Maxwell and Wagner two-layer model [25,26], space charge polarization is caused by inhomogeneous dielectric structure in the material. It is formed by large number of well conducting grains separated by thin poorly conducting intermediate grain boundaries. Rabinkin and Novikova [27] pointed out that polarization in ferrites is similar to that of conduction. By electron hopping between a ferrous ion and a ferric ion, the local electron displacement occurs in the direction of applied field that determines the polarization. At high frequency electron exchange between Fe^{2+} and Fe^{3+} ions does not follow the applied field, which causes a decrease in the contribution of interfacial polarization. Thus, the dielectric constant decreases at high frequency.

Fig. 5 shows an increase in the dielectric constant with increase in sintering temperatures which can be attributed to decrease in porosity at higher sintering temperatures. The pores interrupt the buildup of space charge resulting to a decrease in polarization. Hence, the dielectric constant increases with an increased sintering temperature.

Fig. 6 shows the variation in dielectric loss of Ni–Zn ferrites sintered at various sintering temperatures. The values of dielectric loss decrease with increase of frequency for ferrites sintered at various temperatures. The dielectric loss arises due to the lag in molecular polarization with respect to a changing electric field in a dielectric medium. At higher frequency, when the dipole orientation cannot

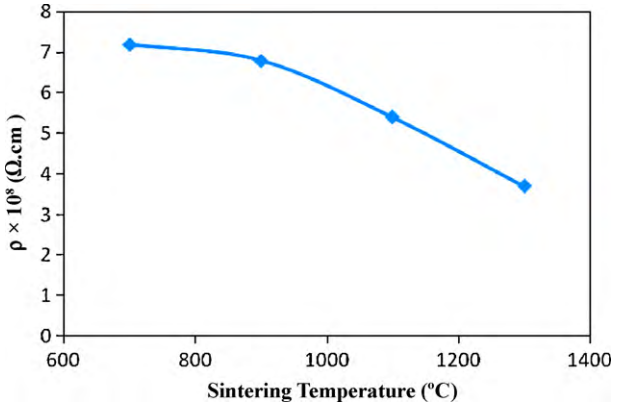

Fig. 4. DC resistivity vs. sintering temperatures.

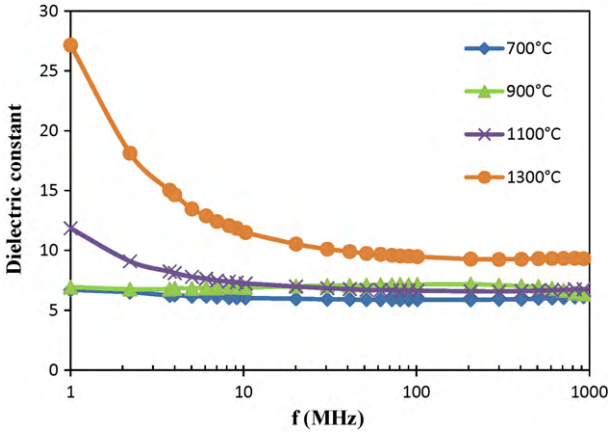

Fig. 5. Frequency dependence of dielectric constant for $Ni_{0.8}Zn_{0.2}Fe_2O_4$.

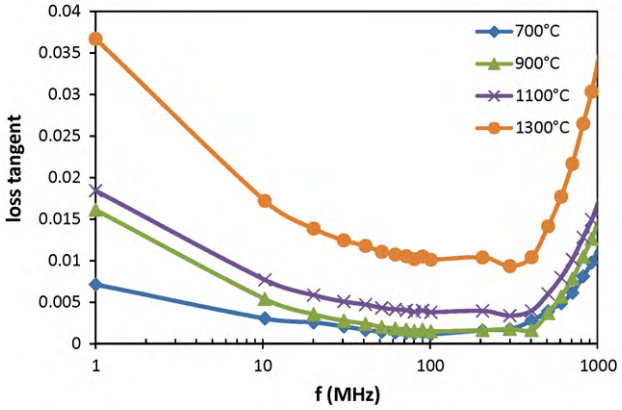

Fig. 6. Frequency dependence of loss tangent for $Ni_{0.8}Zn_{0.2}Fe_2O_4$ prepared via co-precipitation.

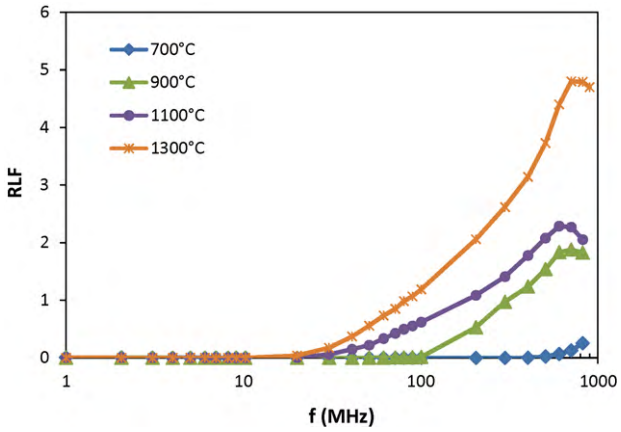

Fig. 8. Relative loss factor vs. frequency for nickel–zinc ferrites.

follow the applied field, the absorption of energy leads to energy dissipation. It is observed that the values of dielectric loss are significantly lower compared to those reported for the ferrites prepared by conventional method [28,29]. None of the samples exhibit a high loss peak within the measured frequency range. If the period of relaxation equals the period of the alternating field, the maximum dielectric loss would occur. It can be concluded that the frequency at which maximum in loss occurs in these samples is outside the frequency range studied [30]. The low value of loss tangent indicates qualities of the substance for high frequency applications.

3.5. Magnetic behaviour

3.5.1. Permeability

Fig. 7 describes the initial permeability results plotted against the frequency in the range of 1.0 MHz to 1.0 GHz for the $Ni_{0.8}Zn_{0.2}Fe_2O_4$ sintered at different temperatures. It is obvious that the sample sintered at 700 °C gives the lowest initial permeability and the widest range of operating frequencies (1–400 MHz). The sample sintered at 1300 °C, on the other hand, gives the highest value of initial permeability. The initial permeability was found to vary with sintering temperature. The initial permeability is observed to be fairly constant over several order of frequency, rises slightly, and then it falls rapidly. The decrease in permeability implies onset of ferromagnetic resonance. The fairly constant μ_i' values over a large frequency range show the compositional stability and quality of the ferrites prepared by the co-precipitation method. This is a desirable characteristic for various applications such as broadband pulse transformers and wide band read–write heads for video recording.

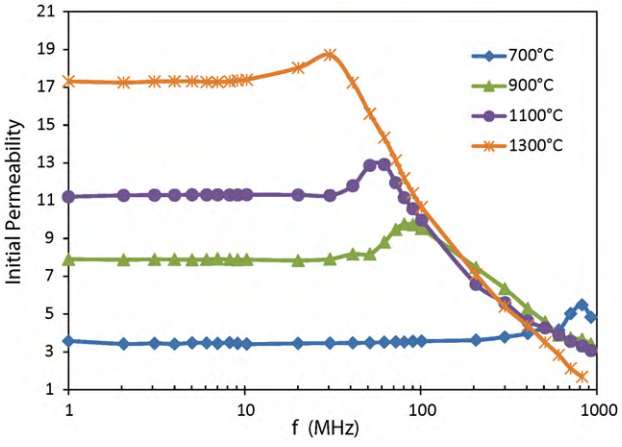

Fig. 7. Initial permeability vs. frequency measured at room temperature for $Ni_{0.8}Zn_{0.2}Fe_2O_4$ for different sintering temperatures.

The initial permeability value lies between 4 and 17 which is lower than that reported [31]. Increase in permeability with sintering temperature can be attributed to increase in density and grain size with sintering temperature [32]. Higher the density and grain size, greater grain-to-grain continuity in magnetic flux leading to higher permeability. Generally, the grain boundaries, local impurities and microstructure defects are relevant for the appearance of the domains with opposite magnetization and for the pinning of domain walls. Thus, the increase in sintered density and diminished grain boundary caused the existence of very mobile domains in the Ni–Zn ferrite. Also during grain growth pores become fewer which act as impediments to domain wall motion due to pinning of the wall.

Furthermore, the increase in the sintering temperature results in a decrease in the magnetic anisotropy by decreasing the internal stress and crystal anisotropy, which reduce the hindrance to the movement of the domain walls [31]. Hence, the initial permeability increased. It is also observed that the higher permeability has a lower resonance frequency. However, a higher initial permeability in this method can be achieved through controlling the grain boundaries, which are dependent on the heat treatment.

The same trend is seen in the case of variation in relative loss factor with respect to frequency as shown in Fig. 8. The RLF values remain constant for all the samples and thereafter rising sharply. The frequency at which the RLF value is minimum, called the threshold frequency, is observed to vary with sintering temperature. The relative loss factor values are observed of the order of 10^{-3} to 10^{-4} in the frequency range of 1.0 MHz to 1.0 GHz. Samples sintered at 700 °C are found to exhibit the lowest RLF values and over a wider frequency range compared to those for samples sintered at higher temperatures (≈400 MHz). This is due to the small grain size. The small grain size means an increase in number of grain boundaries which impedes the eddy current flows. The grain boundary acts as a barrier which functions locally to reduce the hopping of electrons between Fe^{2+} and Fe^{3+} ions in octahedral sites. In the case of samples sintered at higher temperatures, there is a possibility of structural change on account of zinc loss [33] which increases with increasing temperature. The low RLF value indicates the high purity of the samples obtained by the present method.

3.5.2. Hysteresis loop

Hysteresis parameters like coercivity, H_c, residual magnetization, M_r, and saturation magnetization, M_s of $Ni_{0.8}Zn_{0.2}Fe_2O_4$ sintered at different temperatures are listed in Table 4.

Table 4
Hysteresis parameters of $Ni_{0.8}Zn_{0.2}Fe_2O_4$ sintered at different temperatures.

Sintering temperature (°C)	Coercivity, H_c (A m^{-1})	Residual magnetization, M_r (A m^2 kg^{-1})	Saturation magnetization, M_s (A m^2 kg^{-1})
700	5809	8.95	40
900	5411	8.14	53
1100	4456	7.20	56
1300	4138	5.78	63

The measurements were made at room temperature (≈25 °C).

Fig. 9 shows the M–H loop of the $Ni_{0.8}Zn_{0.2}Fe_2O_4$ prepared sample. Obviously, the coercivity decreases by increasing the sintering temperature. This is due to the increase of the average grain size with sintering temperature. The larger grain tends to involve more domain walls. Thus, the contribution of wall movement to magnetization or demagnetization, which required lower energy than domain rotation, increases. Therefore, the larger grains are expected to have low coercivity. A decrease in residual magnetization, M_r, is observed with an increase in sintering temperature. The residual magnetization, M_r, has linear relationship with porosity. Therefore, M_r decreases with increasing sintering temperature.

The magnetization is a result of the simultaneous influence of several intrinsic and extrinsic factors such as density and porosity [33]. The origin of the magnetic moments is responsible for magnetization. The net magnetic moment of the spinel ferrite depends upon the distribution of magnetic ions in A and B sites. As described earlier, the Ni^{2+} ions have unpaired electron spins and prefer the B sites. Therefore, Ni^{2+} ions provide part of the magnetic moment of a spinel. Zn^{2+} is not paramagnetic (no unpaired spin) and occupies the A sites due to the electron configuration exception. Fe^{2+} and Fe^{3+} ions go into both sites, A and B. Zn ions are caused to disproportionate the Fe ions on the crystal lattice sites. Thus, basic magnetic properties of nickel–zinc ferrites come out from Ni^{2+} on the B sites and Fe^{2+} and Fe^{3+} ions on the A sites.

The M_s values depend on the porosity and density. The relation between M_s and porosity and density is expressed by [34]

$$M_s = (1 - P)\delta s d \quad (4)$$

where P is the porosity, d is density and $\delta s = M_s$ (obs)/M_s (sat). From this equation it is clear that the saturation increases with decrease in porosity or increase in density. So, reduction of porosity with sintering temperature could cause M_s increased.

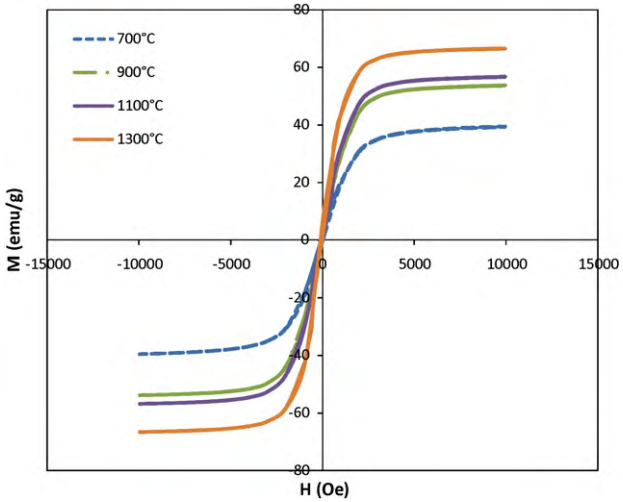

Fig. 9. Hysteresis loops for $Ni_{0.8}Zn_{0.2}Fe_2O_4$ at room temperature.

4. Conclusion

Highly homogeneous Ni–Zn ferrite nanoparticles were prepared by simple and economical chemical co-precipitation method. The presence of Zn^{2+} ions causes appreciable change in the structural, magnetic and electrical properties. The XRD patterns reveal spinel cubic structure for the synthesized materials. The unit cell parameter '*a*' increases linearly with the sintering temperatures from 8.356 to 8.365 Å. The grain size increases with heat treatments, however, much smaller than conventional one. DC electrical resistivity of the samples at room temperature was found to vary from 7.28×10^8 to 3.7×10^8 Ω cm from 700 to 1300 °C sintering temperatures. It has been observed that initial permeability and RLF increase by increasing temperature. The RLF of the samples was low due to the high electrical resistivity. The achievement of this research is increasing the operational frequency range over 400 MHz which is obtained at low sintering temperature (700 °C). The dielectric constant of all the samples decreases with increase in frequency.

Acknowledgement

The authors gratefully acknowledge the Universiti Putra Malaysia for their facility to complete this research.

References

[1] H. Igarash, K. Okazaki, J. Am. Ceram. Soc. 60 (1977) 51–54.
[2] P.I. Slick, in: E.P. Wohlfarth (Ed.), Ferromagnetic Materials, vol. 2, North-Holland Pub. Co., Amsterdam, 1980, p. 196.
[3] T. Abraham, Am. Ceram. Bull. Soc. Bull. 73 (1994) 62–65.
[4] P.S. Anil Kumar, J.J. Shrotri, S.D. Kulkarni, C.E. Deshpande, S.K. Date, Mater. Lett. 27 (1996) 293–296.
[5] A. Verma, T.C. Goel, R.G. Mendiratta, R.G. Gupta, J. Magn. Magn. Mater. 192 (1999) 271–276.
[6] S. Thakur, S.C. Katyal, M. Singh, J. Magn. Magn. Mater. 321 (2009) 1–7.
[7] H. Su, H. Zhang, X. Tang, Y. Jing, Mater. Chem. Phys. 102 (2007) 271–274.
[8] B.D. Cullity, Elements of X-ray Diffraction, 2nd ed., Addison Wesley Pub. Co. Inc., 1978, p. 42.
[9] J. Smit, H.P.J. Wijn, Ferrites, Philips Technical Library, Eindhoven, Netherlands, 1959, p. 150.
[10] E.C. Snelling, Soft Ferrites: Properties and Applications, 2nd ed., Butterworths, London, 1988.
[11] T. Pannaparayil, R. Marande, J. Appl. Phys. 69 (1991) 5349.
[12] M.R. Anantharaman, S. Sindhu, S. Jagatheesan, K.A. Malini, P. Kurian, J. Phys. D 32 (1999) 1801.
[13] J.C. Wurst, J.A. Nelson, J. Am. Ceram. Soc. 55 (1972) 109.
[14] T. Kodama, T. Itoh, M. Tabata, Y. Tamaura, J. Appl. Phys. 69 (1991) 5915.
[15] Y.H. Han, J.J. Suh, M.S. Shin, S.K. Han, J. Phys. IV France 7 (1997), C1-111–C1-112.
[16] S.-i. Pyun, J. -t. Back, Am. Ceram. Soc. Bull. 64 (1985) 602.
[17] A.A. Sattar, H.M. El-Sayed, K.M. El-Shokrofy, M.M. El-Tabey, J. Appl. Sci. 5 (2005) 162–168.
[18] A.B. Naik, J.I. Powar, Ind. J. Pure Appl. Phys. 3 (1985) 436–437.
[19] M. Lal, D.K. Sharma, M. Singh, Ind. J. Pure Appl. Phys. 43 (2005) 291.
[20] L.G. Van Uitert, J. Chem. Phys. 23 (1955) 1883.
[21] K. Iwauchi, Jpn. J. Appl. Phys. 10 (1971) 1520–1528.
[22] G.C. Jain, B.K. Das, R.B. Tripathi, R. Narayan, IEEE Trans. Magn. 18 (1982) 776–778.
[23] R.V. Mangalaraja, S. Ananthakumar, P. Manohar, J. Magn. Magn. Mater. 253 (2002) 56–64.
[24] D. Ravinder, K.V. Kumar, Bull. Mater. Sci. 24 (2001) 505.
[25] J.C. Maxwell, Electricity and Magnetism, Oxford University Press, Oxford, 1873.
[26] K.W. Wagner, Ann. Phys. 40 (1913) 817.
[27] I.T. Rabinkin, Z.I. Novikova, Izv. Acad. Nauk USSR Minsk. (1960) 146.
[28] B. Parvatheeswara Rao, K.H. Rao, J. Mater. Sci. 32 (1997) 6049–6054.
[29] A.M. Abdeen, J. Magn. Magn. Mater. 192 (1999) 121.

[30] R.G. Kharabe, R.S. Devan, C.M. Kanamadi, B.K. Chougule, Smart Mater. Struct. 15 (2006) N36–N39.
[31] A. Verma, T.C. Geol, R.G. Mendiratta, J. Magn. Magn. Mater. 208 (2000) 13–19.
[32] T. Nakamura, Y. Okaro, J. Appl. Phys. 79 (1996) 7129.
[33] A. Verma, O.P. Thakur, C. Prakash, T.C. Goel, R.G. Mendiratta, Mater. Sci. Eng. B 116 (2005) 1–6.
[34] P.K. Maskar, S.V. Kakatkar, R.S. Patil, V.A. Jadhav, N.D. Chaudhari, A.M. Sankpal, S.R. Sawant, Mater. Chem. Phys. 41 (1995) 154–157.